



**HAL**  
open science

## Customizable patterned membranes for cardiac tissue engineering: A model-assisted design method

Bertrand Guibert, Aurelia Poerio, Lisa Nicole, Julia Budzinski, Mélanie Leroux, Solenne Fleutot, Marc Ponçot, Franck Cleymand, Thierry Bastogne, Jean-Philippe Jehl

### ► To cite this version:

Bertrand Guibert, Aurelia Poerio, Lisa Nicole, Julia Budzinski, Mélanie Leroux, et al.. Customizable patterned membranes for cardiac tissue engineering: A model-assisted design method. *Journal of the mechanical behavior of biomedical materials*, 2025, 162, pp.106815. 10.1016/j.jmbbm.2024.106815 . hal-04839358

**HAL Id: hal-04839358**

**<https://hal.science/hal-04839358v1>**

Submitted on 22 Dec 2024

**HAL** is a multi-disciplinary open access archive for the deposit and dissemination of scientific research documents, whether they are published or not. The documents may come from teaching and research institutions in France or abroad, or from public or private research centers.

L'archive ouverte pluridisciplinaire **HAL**, est destinée au dépôt et à la diffusion de documents scientifiques de niveau recherche, publiés ou non, émanant des établissements d'enseignement et de recherche français ou étrangers, des laboratoires publics ou privés.

# Customizable patterned membranes for cardiac tissue engineering: a model-assisted design method

Bertrand Guibert<sup>1</sup>, Aurelia Poerio<sup>1</sup>, Lisa Nicole<sup>1</sup>, Julia Budzinski<sup>3</sup>, Mélanie M. Leroux<sup>1</sup>, Solenne Fleutot<sup>1</sup>, Marc Ponçot<sup>1</sup>, Franck Cleymand<sup>1</sup>, Thierry Bastogne<sup>2,3</sup>, and Jean-Philippe Jehl<sup>1</sup>

<sup>1</sup>Institut Jean Lamour, UMR 7198 CNRS, Université de Lorraine, Nancy, France

<sup>2</sup>CRAN, UMR 7039 CNRS, Université de Lorraine, Nancy, France

<sup>3</sup>CYBERNANO, Nancy, France

## Abstract

Myocardial infarction can cause irreversible damage to the heart muscle, which can lead to heart failure. The difficulty of the treatment mainly arises from the anisotropic behavior of the myocardium fibrous structure. Patches or cardiac restraint devices appear to be a promising approach to post-infarction treatment. In this study, we propose a new model-assisted method to design patterned membranes. The proposed approach combines computer experiments and statistical models to optimize the design parameters and to meet the requirement for the post-infarction treatment. Finite element model, global sensitivity analysis, random forest model and response surface model are the key components of the strategy implemented in this study, which is applied to design a real membrane. The metamodel-based design method is able to estimate the equivalent Young's modulus of the membrane in a few seconds and optimization results have been validated *a posteriori* by laboratory measurements. This solution opens up new prospects for the design of customized membranes with technical specifications tailored to each patient.

*Keywords:* cardiac membrane; mechanical behavior; finite element model; computer experiment; sensitivity analysis; statistical model.

## 1 Introduction

Cardiovascular disease, particularly myocardial infarction, is the leading cause of death worldwide [1]. When a heart attack occurs, there is a total or partial interruption of the

blood supply to part of the heart, resulting in an imbalance between oxygen supply and demand [2]. This leads to a stiffening of this area of the myocardium, which, in turn, modifies the cardiac behavior leading to a mechanical adaptation of the heart known as pathological ventricular remodeling. This is a complex multiscale process [3] which, macroscopically, results in changes in the size and shape of the heart, as well as in changes in the systolic and diastolic function. While in the short-term the ventricular remodeling is very efficient, in the long term it can become deleterious, leading to heart failure [4].

Several methods of passive and active assistance ranging from cardiac patches to artificial hearts have been considered over the past years [5]. One of the most promising is cardiac tissue engineering, including 3D printing of patches as passive mechanical aids that can be activated through the inclusion of cells. Passive devices, which can either surround the whole heart or locally reinforce the infarcted zone, aim to physically limit the pathological dilation of the ventricle and, possibly, to reverse a dilation that has already occurred [1, 6].

The orientation of the fibers in the cardiac tissue varies through the thickness of the muscle (epicardium, myocardium, and endocardium) and vertically from the base to the apex. This unique microstructure induces a particular twisting movement during the cardiac cycle [7], resulting in an anisotropic mechanical behavior and more particularly to local transverse isotropy (local reference frame associated with the fibers) [8].

This anisotropy is one of the most important factors to be considered for the design of passive cardiac patches. However, there is a lack of homogeneity concerning the mechanical properties of the cardiac tissue according to the different studies, which can be attributed to different factors. The first issue is the influence of the phase of the cardiac cycle at which the mechanical properties of the tissue are measured [9]. In fact, the mechanical stresses at which the muscle undergoes during the diastole and systole differs completely, which can lead to different interpretations depending on the moment in the cycle when the heart is being studied. The second factor is the characterization method used [9]. In fact, some of them such as tensile or shear rheometric tests, enable a macroscopic characterization at tissue level, while others, such as nano-indentation, provide more local characterization at the level of a fiber bundle. The final factor is the influence of the area selected for characterization. In fact, each part of the heart has a different stiffness and a different orientation of the fibers, leading to different mechanical properties. Engelmayer G.C. et al. in [10] characterized the two ventricles by tensile test and showed that each is characterized by two Young's moduli, one defined along the longitudinal axis (Apex-base) of the heart and the other along the circumferential axis. According to their results, the left ventricle has a circumferential and longitudinal Young's modulus of  $157 \pm 14$  kPa and  $84 \pm 8$  kPa, respectively, while the right ventricle by  $54 \pm 8$  kPa and  $20 \pm 4$  kPa respectively. Secondly, within each ventricle, the wall thickness and the fiber orientation vary between the base and the apex. These differences within a ventricle must be considered in the development of cardiac patches at a very precise level [8]. In fact, when applied to the heart, the patch must provide the mechanical support it needs, limiting pathological remodeling while avoiding being harmful to the heart by applying undesirable constraints [5]. With this in mind, various materials and manufacturing methods have been and continue to be studied. Cardiac membranes and/or patches can be made from synthetic or natural materials, or sometimes a combination of the two to form hybrid materials, each type having its advantages and disadvantages [11].

One of the aspects we would like to further develop is the use of numerical models and

simulations to speed up the design of new membranes with appropriate and customizable characteristics. This would reduce the need for experimental manufacturing and testing, which can be costly in terms of time and resources. The use of numerical models could help to converge more rapidly on the most promising prototypes. Indeed, numerical simulation models are increasingly being studied and developed for this type of medical device [1, 5, 12, 13, 14].

In a previous study [15], we highlighted a method of manufacturing patterned membranes by the 3D printing of biomaterials, and more precisely a hydrogel of guar gum, chitosan and gelatin, with an equivalent Young's modulus that differs according to the direction of traction. On this basis, we also developed a fully customizable numerical simulation model for tensile testing that can predict the equivalent Young's modulus of these membranes as a function of the printed pattern.

To take the development of a fully customizable and predictive numerical model a step further, this study proposes the a model-assisted design method combining finite element models, global sensitivity analysis and statistical metamodeling to optimize the design parameters of a membrane and to meet the personalized specifications of the targeted membrane. To this end, finite element modelling was used to simulate tensile tests on membranes with different internal patterns and different material properties. A global sensitivity analysis was carried out on the simulation data to identify the most important design parameters. In a third step, the simulation data are used to determined a statistical metamodel able to compute more quickly the possible geometries of the membrane that would meet technical requirements on the equivalent Young's modulus. This engineering approach would allow surgical practitioners, medicines, or medical researchers to quickly determine the most promising patterns and materials to design a membrane able to meet the mechanical specification and adapted to the patient's cardiac deficiency. Such a predictive design paradigm would enable rapid progresses in the field of tissue engineering, particularly in cardiac medicine but not only, with for example possible applications in urinary, gastrointestinal and muscular medicine.

## 2 Materials and methods

### 2.1 Strategy

The singular behavior of the heart reveals the need of designing membranes with mechanical characteristics matching the ones of the heart. At the scale of a fiber bundle, the mechanical behavior is considered as transversely isotropic when the fibers share the same orientation, transitioning to anisotropic when the orientation varies among the fibers. For our study, we treat this anisotropy as orthotropic. This facilitates the correlation between the mechanical characterization of the area of the heart where the membrane is applied and the mechanical characterization of the membrane. From a macroscopic perspective, this implies that the myocardium is viewed as locally orthotropic, indicating distinct mechanical behaviors along its three directions: longitudinal (along the Apex-Base axis), circumferential, and radial (through the thickness of the myocardium). The radial behavior of the myocardium and of the membrane are neglected in this study.

Two different strategies could be used to develop membranes with orthotropic mechanical

properties. The first one is based on the use of composite materials, i.e. a heterogeneous assembly or mixture of at least two components with complementary mechanical properties. The second one is based on the modification of the geometry (pattern) of the membrane in order to modulate its mechanical properties by using a single isotropic material. The latter method is the one explored in this study. In order to determine the mechanical characteristics of an orthotropic material made of isotropic material, we assume the equivalence between a solid membrane made of an orthotropic material governed by the equation (1) and a patterned membrane made of an isotropic material governed by the equation (2). The following equations are defined in an orthonormal basis ( $e_1, e_2, e_3$ ).

$$\epsilon = D\sigma \Leftrightarrow \begin{pmatrix} \epsilon_{11} \\ \epsilon_{22} \\ \epsilon_{33} \\ 2\epsilon_{12} \\ 2\epsilon_{13} \\ 2\epsilon_{23} \end{pmatrix} = \begin{pmatrix} \frac{1}{E_{11}} & \frac{-\nu_{21}}{E_{22}} & \frac{-\nu_{31}}{E_{33}} & 0 & \dots & 0 \\ \frac{-\nu_{12}}{E_{11}} & \frac{1}{E_{22}} & \frac{-\nu_{32}}{E_{33}} & \vdots & \dots & \vdots \\ \frac{-\nu_{13}}{E_{11}} & \frac{-\nu_{23}}{E_{22}} & \frac{1}{E_{33}} & \vdots & \dots & \vdots \\ 0 & \dots & 0 & \frac{1}{G_{12}} & 0 & 0 \\ \vdots & \vdots & \vdots & 0 & \frac{1}{G_{13}} & 0 \\ 0 & \dots & 0 & 0 & 0 & \frac{1}{G_{23}} \end{pmatrix} \begin{pmatrix} \sigma_{11} \\ \sigma_{22} \\ \sigma_{33} \\ \sigma_{12} \\ \sigma_{13} \\ \sigma_{23} \end{pmatrix} \quad (1)$$

With  $\epsilon$  the strain vector,  $D$  the compliance matrix and  $\sigma$  the stress vector. Here, 9 parameters define the compliance matrix, corresponding to the following definitions:

- $E_{ii}$  corresponds to the ratio between the uniaxial stress and the uniaxial strain in the direction of the base vector  $e_i$ .
- $\nu_{ij}$  corresponds to the negative ratio between the axial strain in the  $e_j$  direction and the axial strain  $e_i$  when the material is uniaxially stretched in the  $e_i$  direction.
- $G_{ij}$  is the ratio of the shear stress  $\sigma_{ij}$  to the engineering shear strain  $2\epsilon_{ij}$  in the plane defined by  $e_i$  and  $e_j$ .

$$\epsilon = D\sigma \Leftrightarrow \begin{pmatrix} \epsilon_{11} \\ \epsilon_{22} \\ \epsilon_{33} \\ 2\epsilon_{12} \\ 2\epsilon_{13} \\ 2\epsilon_{23} \end{pmatrix} = \begin{pmatrix} \frac{1}{E} & \frac{-\nu}{E} & \frac{-\nu}{E} & 0 & \dots & 0 \\ \frac{-\nu}{E} & \frac{1}{E} & \frac{-\nu}{E} & \vdots & \dots & \vdots \\ \frac{-\nu}{E} & \frac{-\nu}{E} & \frac{1}{E} & 0 & \dots & 0 \\ 0 & \dots & 0 & \frac{1}{G} & 0 & 0 \\ \vdots & \vdots & \vdots & 0 & \frac{1}{G} & 0 \\ 0 & \dots & 0 & 0 & 0 & \frac{1}{G} \end{pmatrix} \begin{pmatrix} \sigma_{11} \\ \sigma_{22} \\ \sigma_{33} \\ \sigma_{12} \\ \sigma_{13} \\ \sigma_{23} \end{pmatrix} \quad (2)$$

When going from orthotrope to isotrope the number of parameters is reduced from 9 to 2:

- $E$  corresponds to the ratio between stress and strain in a uniaxial tensile test.
- $\nu$  is the negative ratio between transverse strain and axial strain in a uniaxial tensile test.
- $G$  is defined with  $E$  and  $\nu$  by the relation:  $G = \frac{E}{2(1+\nu)}$ .

This reduction in the number of parameters simplifies the characterization of materials of this type.

COMSOL Multiphysics<sup>®</sup> [16] and Matlab<sup>®</sup> [17] were used respectively to predict the deformation of the membranes in a defined tensile direction and to calculate the equivalent Young's modulus of each membrane. The Rstudio<sup>®</sup> software was used for statistical analysis, which enabled us to obtain a model of the various possible combinations of parameters for a given membrane corresponding to the user's request. A summary diagram representing this strategy is shown in Figure 1.

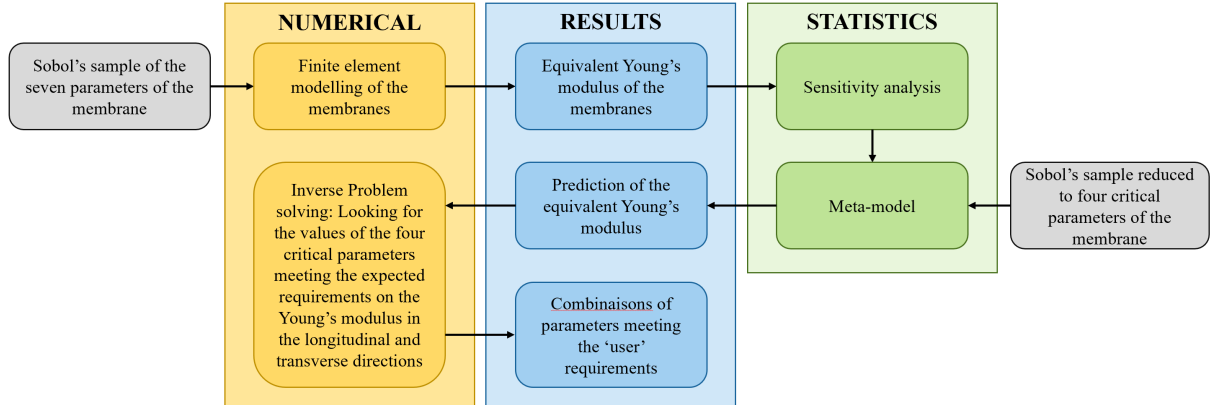


**Figure 1.** Schematic representation of global study strategy.

## 2.2 Finite element model for simulation

The model developed for this study is based on the simulation of a tensile test on a membrane allowing the determination of its equivalent Young's modulus in the tensile direction.

### 2.2.1 Finite element model parameters

The patterned membrane consists of a pavement of rectangular pores extruded from a full rectangular parallelepiped membrane as shown in Figure 2. The numerical model consists of 12 parameters listed in Table 1. Of these 12 parameters, 7 can be customized in order to modify the membrane, of which 4 define the geometry of the membrane and 3 define the material.

The 4 parameters defining to the geometry are the membrane thickness ("em"), the filament width ("fw"), the pore width ("pw") and the pore length ("pl"), as shown in figure 2. The pore length always represents the pore size in the tensile direction, while the pore width represents the pore size in the direction perpendicular to the tensile direction. The width and length of the membrane depend on fw, pw and pl as well as the number of pores in the membrane. The 3 parameters relating to the material are the Young's modulus ("ym"), the Poisson's ratio ("pr") and the density ("d"), as we consider the material here to be purely elastic with isotropic behavior.

The range of values of these 7 parameters (Table 1) was selected based on the most used

materials composing cardiac patches found in the literature on the needs in terms of mechanical properties of the myocardium [8, 9, 10, 18] and on the limits of 3D bioprinting (pores too large would not allow for the structure to be manipulated efficiently). The number of pores in width and length was kept equal to 7 to ensure the sufficient amount of material to proceed to the tensile test in the two directions.

Name	Description	Value/Range
nf	Strength in Newton	0.1
mt	Membrane thickness in millimeters	0.5-2.5
pl	Pore length in millimeters	0.5-10
pw	Pore width in millimeters	0.5-10
fw	Filament width in millimeters	0.5-2
nl	Number of pores in length	7
nw	Number of pores in width	7
ml	Membrane length in millimeters	$nl*pl+(nl+1)*fw$
mw	Membrane width in millimeters	$nw*pw+(nw+1)*fw$
ym	Young's modulus in Pascal	50000-500000
pr	Poisson's ratio	0.40-0.49
d	Density in kg/m <sup>3</sup>	800-1500

**Table 1.** Table summarising the parameters of the numerical simulation model with the fixed values for some parameters (nf, nl, nw, ml and mw) and the range of values of the 7 parameters which can be customized to fabricate the membranes (mt, pl, pw, fw, ym, pr and d).

### 2.2.2 Modelling the tensile test

In this model, we consider the membrane to be purely elastic with isotropic behavior. As a consequence, in COMSOL Multiphysics<sup>®</sup> [16], we used the linear elastic material component, whose calculations are based on Hooke's law refer in equation 3 [19].

$$\sigma = E\varepsilon. \quad (3)$$

The membrane is constructed by extruding a patterned membrane using the different geometric parameters in Table 1. In real experiments, the membrane undergoing the tensile test is pinched between jaws in order to be held in place. To get as close as possible to this situation, we defined two boundary conditions. The first involves fixing one end of the membrane to a titanium bar, and the second involves fixing the opposite end as embedded. This allows us to avoid using contact and friction laws that complicate the calculations but are not relevant to this study. The parameters of the titanium bar are as follows: a Young's modulus of  $105*10^9$  Pa, a Poisson's ratio of 0.33, and a density of 4940 kg/m<sup>3</sup>. Titanium was chosen for its mechanical properties, which will result in negligible deformation of the fastener bar in relation to the stresses involved.

The displacement of the titanium bar was restricted to the longitudinal tensile direction, to avoid deformation in other directions. The tensile test was then simulated by pulling

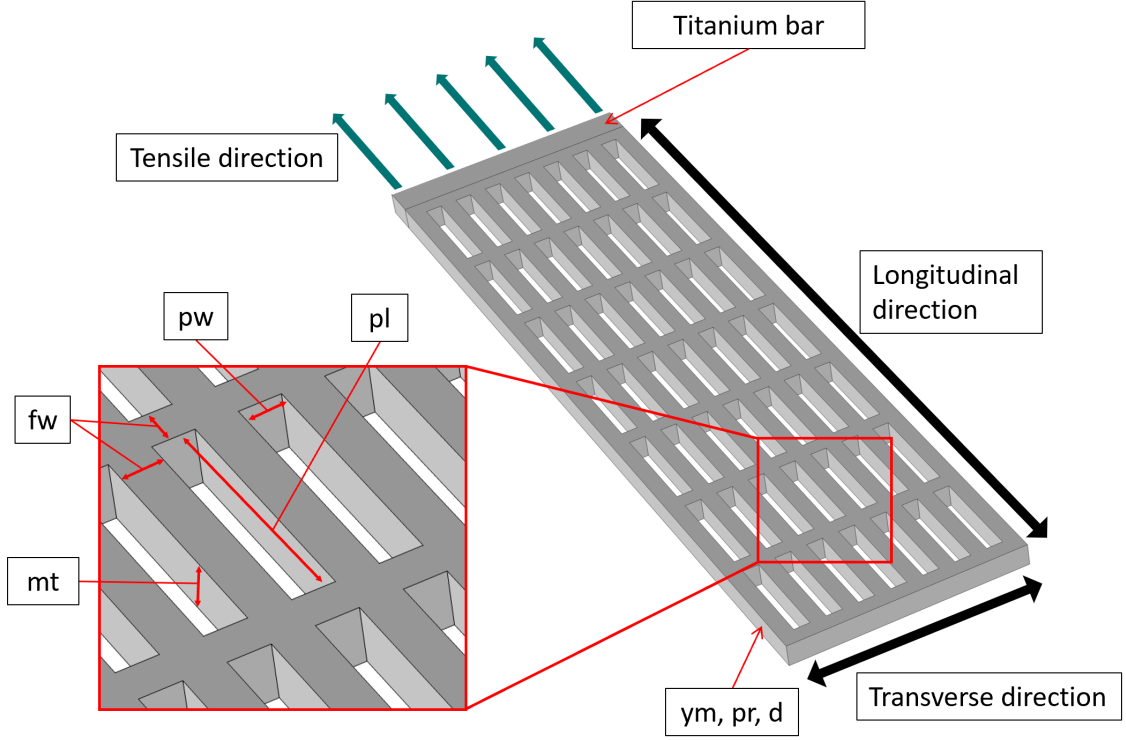


**Figure 2.** Representative image of a patterned membrane showing the customizable parameters and the definition of longitudinal and transverse directions. (mt: membrane thickness, pl: pores length, pw: pores width, fw: filament width, ym: Young's modulus, pr: Poisson's ratio, d: density)

the titanium bar with a total force of 0.1 N, as shown in Figure 2 during 1 second, with increments of 0.1 second.

### 2.2.3 Calculation of the equivalent Young's modulus of the membrane

The equivalent Young's modulus of the membrane with a particular pattern was calculated using the Hooke's Law, described by equation (3), where  $\sigma$ ,  $E$  and  $\varepsilon$  represent respectively the stress, the Young's modulus, and the strain, in a context of pure elasticity. As the equation (3) shows, to obtain the equivalent Young's modulus of the membrane, the directing coefficient of the curve between stress and strain must be determined. These last two are given by the following equations (4) and (5):

$$\varepsilon = \Delta L / l_0, \quad (4)$$

$$\sigma = F / S, \quad (5)$$

where  $\Delta L$ ,  $l_0$ ,  $F$  and  $S$  are respectively the elongation, the initial length, the force and the cross-sectional area of the membrane. The simulation can be used to solve these equations. The elongation is obtained by calculating the displacement norm of a point located at the junction between the membrane and the titanium bar. The initial length and



force are respectively the parameters  $ml$  and  $nf$  in Table 1. Finally, the cross-sectional area is calculated as follows:

$$S = mt \times mw, \quad (6)$$

where  $mt$  and  $mw$  are defined in Table 1.

## 2.3 Statistical metamodel for sensitivity analysis and optimization

### 2.3.1 Sensitivity analysis

Sensitivity analysis is a statistical study that allows us to define which of the seven design 7 parameters have the greatest influence on the characteristic to control: the equivalent Young's modulus of the membrane. The aim is then to only focus on the sensitizing parameters to reduce the computing time and therefore speed up the development of the membrane. To that aim, we applied two different techniques presented below.

#### 2.3.1.1 Sobol sampling

The study of the additive and combined effects of the seven design parameters requires to varying them in an experimental domain corresponding to a 7-dimensional hypercube. The number and location of testing points within this domain determine the duration of the simulations and the accuracy of the final predictions. Sampling strategies for computer experiments is a specific branch in the field of the statistical design of experiments [20, 21, 22, 23]. The Space Filling Designs belong to this category and are particularly well suited to implement global sensitivity analysis [24]. Among the various possible space filling designs, we have implemented thereafter the quasi-random sampling method based on Sobol's sequences [25, 26], using the function *sobolset* in the Matlab software [17]. The result is a sample of 2,800 points in the 7-dimensional space of parameters.

#### 2.3.1.2 Total sensitivity using the Sobol's method

The concept of Global Sensitivity is described in [24] and is attributable to Saltelli [27]. It is an extension of the original approach of Sobol [28] and Homma and Saltelli [29]. This method provides two types of results: single (first-order) and total sensitivity indices, as illustrated in the appendix A. These two indices vary between 0 and 1, where 0 means the parameter has no influence and 1 meaning it has a maximal effect. The first-order sensitivity index  $S_j$  estimates the influence on the response of the  $j$ th parameter alone, while the total sensitivity index  $S_{T_j}$  takes its potential interactions with the other parameters into account.

#### 2.3.1.3 Sensitivity using random forests

To corroborate the results obtained by the previous method, random forests were used. A Random Forest is a specific machine learning method that is used for both classification and regression tasks [30]. It combines multiple decision trees to make more accurate predictions and improve generalization. In order to evaluate the influence of each parameter on the equivalent Young's modulus we used the permutation of the Out-Of-Bag (OOB) data. The

OOB data is defined as the data not selected in the Bagging phase for the construction of the tree. For each tree, the prediction error on the part of the OOB data is recorded and the same procedure is then followed after permuting each predictor variable. The difference between the two is then averaged over all the trees [30]. The parameter has a greater influence when the difference is larger. Such a method was used in [31] to estimate the variable importance in NMR spectral analysis.

### 2.3.2 Metamodeling based on a generalized linear regression

To avoid using the finite element model, which is time-consuming, a metamodel, i.e. a simplified model of the behavior of the initial simulation model, was used to predict faster the equivalent Young's modulus of the membrane.

The simulation data set, defined in section 2.3.1.1, was divided into two parts. The first one, composed of 80% of the complete dataset, is the training set used to identify the statistical metamodel. The remaining part, 20% of the initial dataset, is the testing set. The metamodel structure relies on a generalized linear model often used for the design of experiment under the name *quadratic response surface model* [32], described as follows:

$$Y = \beta_0 + \sum_{i=1}^k \beta_i X_i + \sum_{i=1}^k \beta_{ii} X_i^2 + \sum_{i=1}^{k-1} \sum_{j=i+1}^k \beta_{ij} X_i X_j + E \quad (7)$$

$Y$  is the variable to be estimated, the equivalent Young's modulus of the membrane here,  $X_i$  is the  $i$ th membrane parameter to test,  $k$  is the number of membrane parameters, the  $\beta_0$ ,  $\beta_i$ ,  $\beta_{ij}$  are the metamodel parameters to be estimated and  $E$  in the modeling error (residual) described by a random variable. The estimation phase was carried out in the R software environment for statistical computing in which the *rsm* function was used to implement the generalized linear regression. This model was finally reduced by removing its less constitutive significant terms.

## 2.4 Customizable development

The primary advantage of this development lies in its ability to customize membrane development, allowing by the computation of all potential geometries and material properties that align with the patient's requirements, i.e. a membrane with specific longitudinal and transverse values of the Young's modulus. To that aim, a new Sobol's space sampling, limited to the parameters selection provided by the sensitivity analysis, was carried out. This sample was built using the function *generate\_sobol\_set* in the *spacefillr* package [33] of the R computing environment.

The metamodel is then applied to each point of the sample to estimate the resulting equivalent Young's modulus. All the estimates are finally gathered in a database in which an algorithm detects which combinations of the membrane parameters meet the requirements related to the longitudinal and transverse Young's moduli with a given error margin.

## 2.5 Experimental validation of the metamodel

To experimentally validate the predictions provided by the previous metamodel, patterned membranes with two different materials were 3D printed. The first one (a hydrogel made of chitosan-guar-gum and gelatin and named CH-Gel-GG) was prepared as already reported in a previous study validating the finite element model (CIT) and whose results are used here to also validate the metamodel. The second one (a hydrogel made of alginate and gelatin and named Alg-Gel) was prepared as following. Sodium alginate (Sigma-Aldrich ; MW included between 12000 and 40000 g/mol ; CAS 9005-38-3) and porcine gelatin (Honeywell ; CAS 9000-70-8) were dissolved in water at a weight ratio of 20/80 and placed in an oven (40°C) under constant stirring for at least 1 hour. The resulting ink was then loaded into a syringe and bioprinted with a 4th generation 3D-Bioplotter from EnvisionTEC. The syringe temperature controller was adjusted at 26 °C and a computer-aided design (CAD) software was used to design two different structures using a 250 µm inner diameter needle, a speed of 20 mm/s and a pressure of 1.1 bar. The membranes were created by printing 10-layer membranes with alternated (90°) vertical and horizontal filaments in order to create an internal pattern made of rectangles with a longitudinal or transverse orientation with respect to the overall rectangular structure of the membrane. The distance between filaments was kept at 7.7 mm for the vertical direction and 2 mm for the horizontal direction (longitudinal membranes) and vice versa (transverse membranes). In order to create the full membranes (which allows to obtain the values of Young’s modulus of the bulk material) the ink was poured into a mold with the same external shape as the 3D printed membranes. After printing and after molding, the samples were immersed in a solution made of ethanol and NaOH (for CH-Gel-GG) or in a solution of 2% of CaCl<sub>2</sub> (for Alg-Gel) for 30 min, washed 3 times with PBS and incubated overnight in PBS at 37 °C before performing the tensile tests. The mechanical properties of both CH-Gel-GG and Alg-Gel membranes (both full and patterned) were investigated via uniaxial tensile test. The test was performed using an MTS 4/ML tensile machine equipped with 100 N load cell at room temperature at a constant speed of 2 mm/min. The findings are reported through stress-strain curves and the average Young’s modulus (kPa) along with the standard deviation, for multiple independent membranes. The experimental Young’s modulus was determined as the slope of the linear region observed in the stress–strain curve. Other values (filament width, pore length and pore width) were measured on pictures of the membranes by using the software image J. The slight difference between theoretical and experimental values of the above-mentioned parameters are due to the shrinkage of the material after gelation (in ethanol and NaOH).

## 3 Results

### 3.1 Analysis of raw data

Figure 3 shows the equivalent Young’s modulus of the membranes ( $e_{ym}$ ) computed with the FEM model for all the combinations of the 7 studied parameters involved in the Sobol’s sample 2.3.1.1. The higher the gradient of color in the graph (representing the equivalent Young’s modulus), the higher is the influence of the variable. To facilitate the visualization, the graphs are grouped by the parameters defined in the x-axis (in the order: mt, pl, pw, fw,

d and  $y_m$ ). As shown in figure 3, the variables  $y_m$ ,  $p_w$ , as well as  $f_w$  to a lesser extent, seem to have the greatest impact on the equivalent Young’s modulus, while the others ( $d$ ,  $p_r$ ,  $m_t$  and  $p_l$ ) seem to only have a very negligible effect. For instance, by looking at the graph Poisson’s ratio ( $p_r$ ) as function of the Young Modulus ( $y_m$ ), the gradient of color along the x-axis indicates an influence of the Young’s modulus, while the absence of gradient along the ordinate axis indicates the absence of influence of the Poisson’s ratio. As another example, by looking at the Young’s modulus of the material ( $y_m$ ) as a function of pore width ( $p_w$ ), a diagonal gradient of colors along the two axes appears indicating the influence of the two parameters.

### 3.2 Sensitivity analysis

The equations (A.2) and (A.3) were used to compute the first-order sensitivity and total effect indices. As shown in Figure 4 (A.1) and (A.2), according to the Sobol’s method, the three most critical parameters are: the Young’s modulus of the material ( $y_m$ ), the pore width ( $p_w$ ), and the filament width ( $f_w$ ). To confirm those results, another method based on random forests was used as described in section 2.3.1.3. The method gave similar results, as it can be seen in Figure 4 (B.1) and (B.2). It confirms the three most important variables are the Young’s modulus of the material, the pore width and the filament width.

### 3.3 Statistical metamodel

The material Young’s modulus, the pore width and the filament width were used as regressors in a statistical metamodel as described in section 2.3.2. Since membranes are designed to have an orthotropic mechanical behavior, they have two equivalent Young’s moduli depending on the traction direction: a longitudinal and a transverse equivalent Young’s modulus.

For the longitudinal modulus, the three most important variables are  $y_m$ ,  $p_w$ ,  $f_w$ , whereas for the transverse modulus they become  $y_m$ ,  $p_l$ ,  $f_w$ , because the pore width in one direction of traction becomes the pore length in the other one and *vice versa*. Consequently, the metamodel has four variables: Young’s modulus of the material, pore width, pore length and filament width. The method described in the section 2.3.2 was applied to estimate the metamodel coefficients. To avoid possible negative predictions, the output variable of the metamodel is the logarithm transformation of the equivalent Young’s modulus. After removing insignificant terms, the final metamodel has still very good fitting performances with an adjusted coefficient of determination:  $R_a^2 \approx 0.9923$ , and an average prediction error of 5.15% on the testing set. The metamodel coefficients are presented in Table 3 in Appendix B. All have p-values less than  $2.2e-16$ . A Kolmogorov-Smirnov test was performed with a non-significant result (p-value = 0.1104) justifying the use of this generalised linear model.

### 3.4 Experimental validation of the metamodel

To validate the metamodel, the experimental results were compared with those predicted by the metamodel. More in detail, we performed tensile test on two types of patterned membranes (one corresponding to the longitudinal and one to the transverse orientation of the fibers) made of two different materials (either CH-Gel-GG or Alg-Gel). The experimental



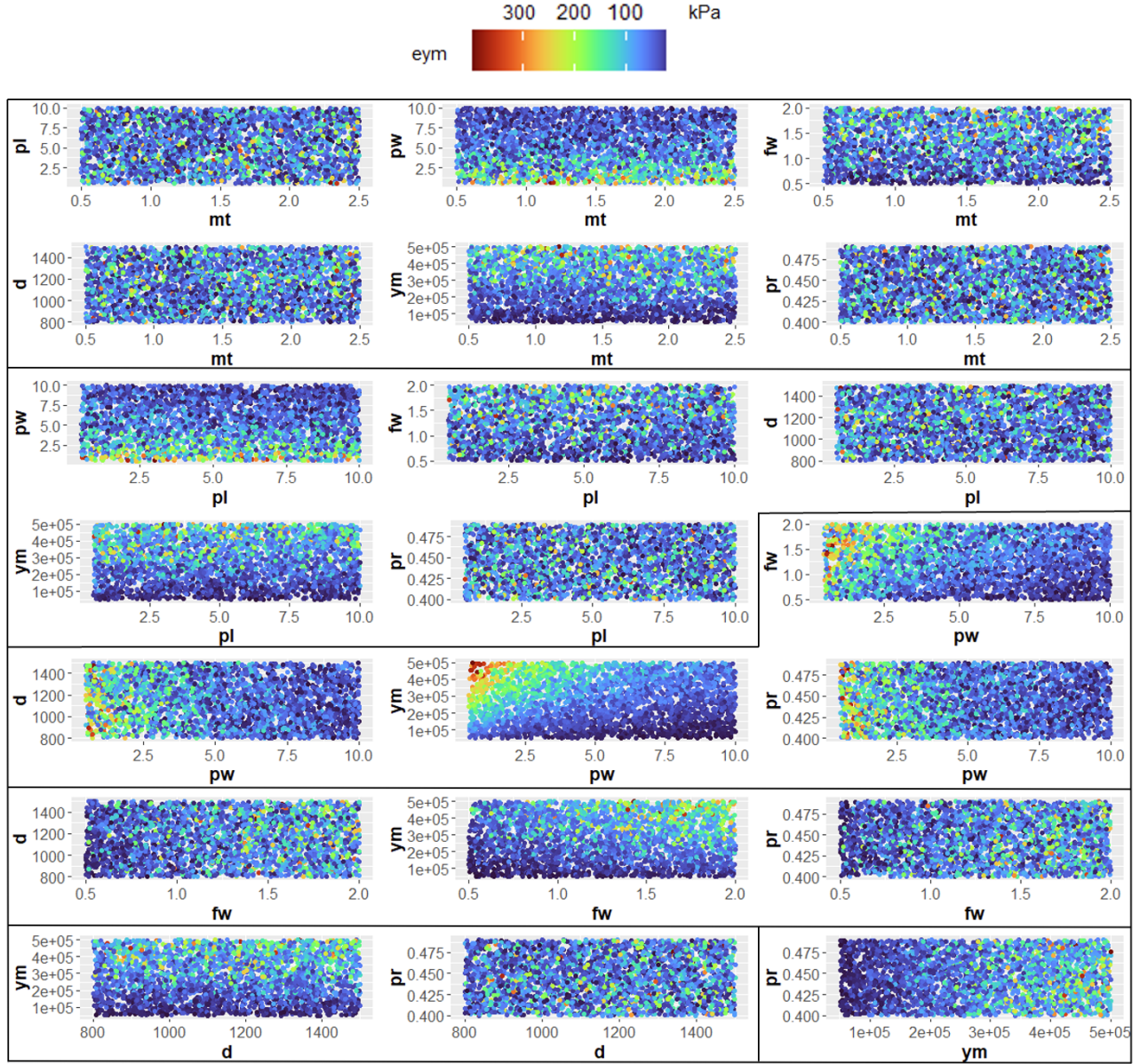


**Figure 3.** Raw data representations of the equivalent Young's modulus ( $e_{ym}$ ) calculated using the FEM model 2.2 and the method described in the section 2.2.3 as a function of pairwise combinations of all parameters. (mt: membrane thickness (mm), pl: pores length (mm), pw: pores width (mm), fw: filament width (mm), ym: Young's modulus (Pa), pr: Poisson's ration, d: density ( $\text{kg}/\text{m}^3$ ),  $e_{ym}$  : equivalent Young's modulus (kPa)). The graphs are grouped by the parameters defined in the abscissa.

results (a pair of equivalent Young's moduli for the longitudinal and transverse orientation of the fibers) obtained for the patterned membranes are then used in order to conduct a research within the metamodel. A representation of the tensile test is shown in Figure 5(A) and quantitative results of the tensile tests are reported in Figure 5(B) and Table 2. Concerning the membranes made of CH-Gel-GG, the Young's modulus of the material (full

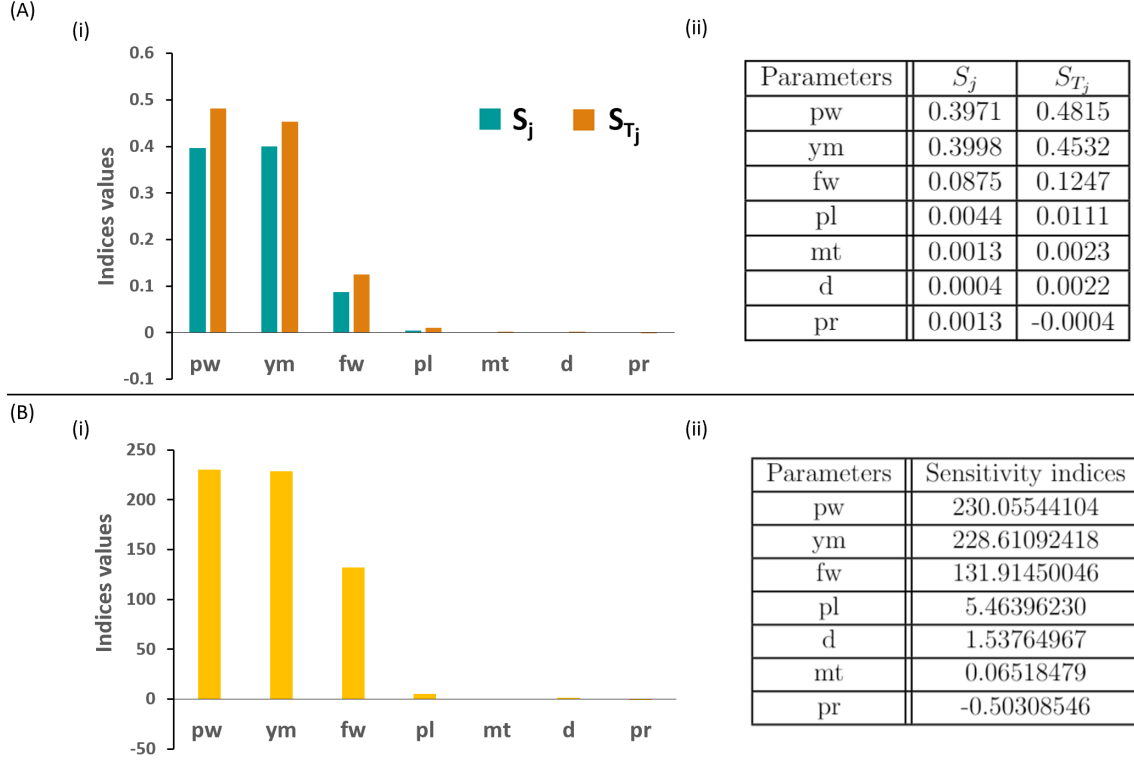


**Figure 4.** Results of the sensibility analysis of (A) Sobol and (B) the random forest. (A.i) Graph representing the Sobol’s indices of sensibility with the first-order sensitivity indices  $S_j$  and the total sensitivity indices  $S_{T_j}$ . (A.ii) Table representing the Sobol’s indices of sensibility. (B.i) Graph representing the sensitivity indices calculated from the permutation of OOB data in the random forest. (B.ii) Table representing the sensitivity indices calculated from the permutation of OOB data in the random forest. (mt: membrane thickness, pl: pores length, pw: pores width, fw: filament width, ym: Young’s modulus, pr: Poisson’s ration, d: density)

membrane) was found to be  $92.27 \pm 8.58$  kPa, while the longitudinal/transverse Young’s moduli were found to be  $(46.17 \pm 2.50$  kPa/ $19.76 \pm 2.16$  kPa). All the other data were also measured experimentally (i.e. the filament width, the pore length and pore width (first line in Table 2). The great potential of the metamodel is that when searching for the possible combinations of materials and patterns resulting in a pair of equivalent Young’s moduli of  $46.2 \pm 2$  and  $19.8 \pm 2$  kPa (error selected by the user) it gives us 1438 different possible combinations (Figure 5(C) where each point represent a combination of materials and patterns resulting in the requested pair of equivalent Young’s moduli). Among them, one combination closely matches the experimental values of Young’s modulus of the material, filament width, pore length and pore width (second line of Table 2 and black point in Figure 5(C)). In the third and fourth line of Table 2, we showed two other examples of combinations that still correspond to the pair of equivalent Young’s moduli. However, we can notice that the values of Young’s moduli and of the patterns (fw, pl and pw) are extremely different with either very large pores and thin filaments (line 3) or vice-versa (line 4). In order to show the robustness of the method, the second part of the Table 2 and the figure 5(D) shows the same process but this time applied on Alg-gel membranes. In this case the pair of equivalent

Young's modulus was  $95.3 \pm 2$  kPa/ $42 \pm 2$  kPa and the number of possible combinations resulting from the metamodel was 570.

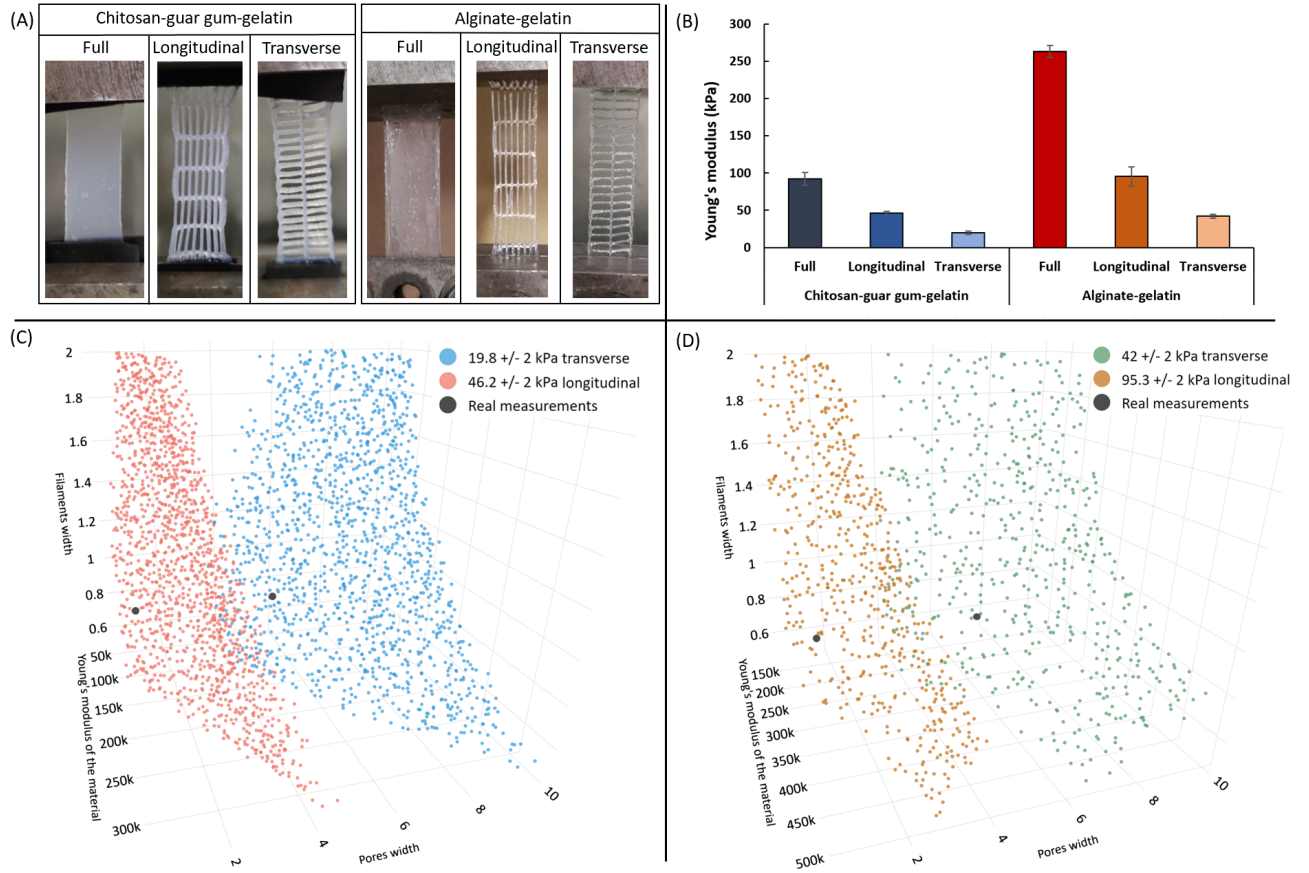


**Figure 5.** (A) Photographs of a full membrane, a membrane with vertically oriented pores and a membrane with pores of the same size oriented horizontally of each material (chitosan-guar gum-gelatin and alginate-gelatin) during the tensile test. (B) Average Young's modulus calculated from the linear region of the stress-strain curve, on five independent membranes for each condition. (C) Graph showing the combinations predicted by the metamodel for the pair of the equivalent Young's moduli of  $46.2 \pm 2$  kPa/ $19.8 \pm 2$  kPa (longitudinal in red and transverse in blue experimentally measured for chitosan-based membranes with the geometrical parameters defined in Table 2. (D) Graph showing the combinations predicted by the metamodel for the pair of the equivalent Young's moduli of  $95.3 \pm 2$  kPa/ $42 \pm 2$  kPa (longitudinal in brown and transverse in green experimentally measured for alginate-based membranes with the geometrical parameters defined in Table 2. In both graphs (C) and (D), the experimental data are represented by black dots.

A database of 500000 membranes was used, which requires 1000000 combinations of parameters for which the equivalent Young's modulus was estimated ( $500000 \times 2 = 1000000$  as there is the longitudinal and transverse Young's modulus for each membrane). In the case illustrated, we decided to select the results within an arbitrarily chosen interval of  $\pm 2$  kPa around the defined values, this value necessarily influencing the number of resulting combinations of parameters. Note that this interval is fully adjustable by the user. In Figure 5, all the points are matched two by two because here we are representing only the

following 3 parameters: Young’s modulus of the material, filament width and pore width. As the pore width in the longitudinal direction corresponds to the pore length in the transverse direction, each pair of points corresponds to a membrane.

Using the metamodel provides a significant advantage in terms of computational time for computing the equivalent Young’s modulus of the membrane compared to the finite element model. Indeed, while the finite element model takes around  $5 \cdot 10^4$  seconds to estimate the equivalent Young’s modulus for 1,800 parameter combinations, the metamodel allows us to estimate the same modulus for one million combinations from the database in less than 1 second. The calculations were performed on a DELL Precision 7750 computer equipped with an Intel(R) Core(TM) i7-10850H CPU 2.70GHz processor and 32 GB of RAM.









## 4 Discussion

With this study we propose a method to accelerate the development of patterned membranes for medical, but not exclusively, applications. While cardiac tissue is well known as an highly anisotropic tissue, revealing the need to use for its repair cardiac membranes with specific mechanical proprieties, this is also true for other tissues and might as well be useful in other material engineering applications. 3D printing represents a very promising technology for this purpose allowing very easily to create anisotropy, due to its own operating method. However, the optimization of a biomaterial-based ink allowing to create a specific pattern can be time consuming. Similarly, characterizing by tensile test even a small part of all the possible combinations of materials and patterns that would result in the desired values of Young’s moduli in the selected direction is not only time consuming but can also be extremely expansive. As a consequence, we showed in this study our strategy to numerically perform these tests and reduce the experimental time. The first stage of the study was to develop a database using a finite element numerical simulation model of membranes. These membranes have specific patterns, which enables their mechanical behavior to be differentiated according to the direction in which the stresses are applied. Secondly, this database is used to develop a statistical metamodel of the finite element model. This is used to visualize the potential mechanical characteristics of these membranes and to characterize the geometric and material variables required to obtain them.

A global sensitivity analysis was conducted to determine the most influent parameters in our FEM model affecting the equivalent Young modulus of the membrane. This method was used to allow us to restrain and focus the study exclusively on the most relevant parameters. Despite an inconsistency on the value of the total Sobol’s indice of the Poisson’s ratio ( $\nu$ ), the results obtain by the sensitivity analysis seems consistent with the analysis of the raw data and was confirmed by the random forest method. According to Saltelli’s formulation [24], the negative value can possibly be justified by the calculation method, probably because of the uncertainty of the calculation. Moreover, this value is tiny and close to zero, so the influence of this parameter on the equivalent Young’s modulus of a resulting membrane can be considered not significant.

The combinations determined by the algorithm to meet the user’s request (see section 2.4) only consider the parameters of the metamodel (the influent parameters resulting from the statistical study), i.e. the Young’s modulus of the material, the width of the filaments, the



	Parameters				Equivalent Young's modulus (kPa)		Patterns
	ym	pw	pl	fw	Longitudinal	Transverse	
	(kPa)	(mm)	(mm)	(mm)			
Membranes made from a chitosan, gelatin and guar gum hydrogel							
Experimental results	92.27 ± 8.58	1.04	5.58	0.80	46.17 ± 2.50	19.76 ± 2.16	
The closest predicted <i>In silico</i> results	94.73	0.93	4.55	0.81	44.41	18.70	
Other examples of predictions	325.01	4.27	9.53	0.50	46.11	21.53	
	50.46	1.25	5.91	1.98	44.21	19.98	
Membranes made from an alginate and gelatin hydrogel							
Experimental results	263.03 ± 8.02	1.14	6.11	0.83	95.32 ± 12.67	42.03 ± 2.76	
The closest predicted <i>In silico</i> results	266.30	1.92	6.18	0.85	95.84	40.29	
Other examples of predictions	499.37	3.64	9.70	0.79	97.11	42.02	
	114.79	0.50	4.45	1.99	93.42	42.85	

**Table 2.** Table comparing the equivalent Young's moduli of experimental membranes with the predictions of the equivalent Young's moduli by the metamodel. Here two types of membrane are compared: 3D bioprinted membranes with a guar gum, chitosan and gelatin hydrogel on the one hand and an alginate and gelatin hydrogel on the other. The Young's modulus associated with the chitosan-based material 92.3 kPa and with the alginate-based material is 263.03 kPa. The "Patterns" column shows the differences in geometry between the membranes, with the filaments in grey and the pores in black. (mt: membrane thickness, pl: pores length, pw: pores width, fw: filament width)

length and the width of the pores. Because of their limited impact on the equivalent Young's modulus, the other parameters (pr, d, mt) used in the FEM model appear to be modular, provided that they are kept within the ranges defined in the table 1. This modularity allows the user greater freedom in the choice of materials for membrane manufacture.

This method requires the establishment of a fairly large database in order to obtain a sufficiently homogeneous representation of the main parameters. The results obtained depend entirely on this database, which means that everything depends on the size of the sample. Now, as it's described in the section 3.4, the number of parameter combinations differs according to the 'user' demand. Thus, for a database of 500000 parameter combinations for the membrane, we obtain 1438 combinations for Young's modulus conditions of  $19.8 \pm 2$  kPa transversely and  $46.2 \pm 2$  kPa longitudinally, while we obtain 570 combinations for Young's modulus conditions of  $42 \pm 2$  kPa transversely and  $95.3 \pm 2$  kPa longitudinally. The huge gap shows the influence of the sample size on the obtained results.

The elaboration of this type of medical device, with a lot of combinations of parameters, usually requires the use of numerical simulations due to the cost and the time consume by this task. However, as this study shows, even the numerical simulation can be time consuming, especially with big database, requiring the use of more efficient methods. The global sensitivity analysis of Sobol and the metamodel created helped us to resolve this problem by reducing the calculation time and still keeping a quite good precision.

The metamodel allows us to come close to the experimental results, even if, as shown in the Table 2, there are some differences between the "The closest predicted *In silico* results" and the experimental value. These slight differences can be explained by the approximations of the measurements from an experimental point of view, by the assumption of elasticity of the membranes in the FEM model, as well as by the intrinsic variability of the statistical metamodel. Nevertheless, these results validate the metamodel for a prediction that is fairly representative of reality, making it possible to help a user in the design of patterned membranes.

It is important to emphasize that the equivalent Young's modulus in the radial direction of the membrane (which corresponds to the thickness), neglected in our study, is inherently connected to both the longitudinal and transverse Young's moduli. This connection arises because the parameters are determined by the resulting configurations based on the user's request, consequently yielding an equivalent radial Young's modulus for the membrane that varies with each configuration.

## 5 Conclusions and perspectives

In this study, a new model-assisted membrane design method is proposed and tested. A global sensitivity analysis is firstly applied to a finite element model of a patterned membrane to identify which design parameters have the most impactful effects on the equivalent Young's modulus considered as the variable to control. Among seven pre-identified parameters, three appeared during the sensitivity analysis as critical: the Young's modulus of the constitutive material, the pore width, and the filament width. In a second step, the sensitive parameters have been used as regressors in statistical metamodel, itself employed as a fast

way to determine the values of parameters, *i.e.* the various possible geometries of the membrane, able to meet the technical requirements on the targeted equivalent Young’s modulus. The metamodel is based on a second-order response surface polynomial model. A quasi Monte-Carlo sampling method, also known as Sobol’s sampling, was applied to the FEM to constitute a dataset devoted to the estimation and testing steps of the metamodel identification. Simulations based on the metamodel are in average several million times faster than the ones carried out with the finite element model. The proposed approach was applied to the development of a real membrane and the comparison of the predicted properties with the ones measured has confirmed the practical relevance of this approach. However, in this study, the model-based design is limited to the modeling of the equivalent Young’s modulus of the membrane. Consequently, future works will need to investigate applications to other mechanical properties. Moreover, this study assumes the employed materials have a purely elastic behavior. It would still be appropriate to develop this model by considering the complexity of some materials and, by incorporating, for instance, the notion of viscosity which is, a characteristic often intrinsic to biomaterials likely to be used for membranes. Even in the current form, this method would therefore save time when designing anisotropic membranes for medical or other material engineering applications.

## Acknowledgments and funding

The authors wish to thank ASCATIM and CARE FEDER PROJECTS of University of Lorraine, for their valuable participation and support. These projects are financed by the European Union operational program FEDER-FSE Lorraine et massif des Vosges 2014-2020, managed by the Grand Est Region. This work was also supported by the French PIA project ‘Lorraine Université d’excellence’, reference ANR-15-IDEX-04-LUE and within the scope of the UL-International Research Project (French-Portuguese) HOPE and of CNRS GDR 2088 ”BIOMIM”.

## A Global sensitivity analysis of Sobol

This method consists of creating two sets of data, forming 2 matrices, each containing  $k = 7$  columns corresponding to the  $k$  parameters and  $N = 1400$  rows corresponding to the number of draws in the experimental domain  $[0,1]^7$  divided by two to be distributed in each matrix. They are labelled A and B below:

$$A = \begin{pmatrix} a_{1,1} & \cdots & a_{1,j} & \cdots & a_{1,k} \\ \vdots & & \vdots & & \vdots \\ a_{i,1} & \cdots & a_{i,j} & \cdots & a_{i,k} \\ \vdots & & \vdots & & \vdots \\ a_{N,1} & \cdots & a_{N,j} & \cdots & a_{N,k} \end{pmatrix}; \quad B = \begin{pmatrix} b_{1,1} & \cdots & b_{1,j} & \cdots & b_{1,k} \\ \vdots & & \vdots & & \vdots \\ b_{i,1} & \cdots & b_{i,j} & \cdots & b_{i,k} \\ \vdots & & \vdots & & \vdots \\ b_{N,1} & \cdots & b_{N,j} & \cdots & b_{N,k} \end{pmatrix};$$

These two matrices are used to create  $k$  others, one for each parameter, in which combinations of A and B are made. For each parameter  $j$ , a matrix  $C_j$  is defined, in which all the

columns come from B except column  $j$ , which comes from A, as follows:

$$C_j = \begin{pmatrix} b_{1,1} & \cdots & b_{1,j-1} & a_{1,j} & b_{1,j+1} & \cdots & b_{1,k} \\ \vdots & & \vdots & \vdots & \vdots & & \vdots \\ b_{i,1} & \cdots & b_{i,j-1} & a_{i,j} & b_{i,j+1} & \cdots & b_{i,k} \\ \vdots & & \vdots & \vdots & \vdots & & \vdots \\ b_{N,1} & \cdots & b_{N,j-1} & b_{N,j} & b_{N,j+1} & \cdots & b_{N,k} \end{pmatrix}$$

Next, the model presented in section 2.2.2 and the method described in section 2.2.3 are used to calculate the equivalent Young's modulus for all the input values of the sampling matrices A, B and  $C_i$ , for  $i$  ranging from 1 to 7. 9 output vectors are obtained of dimension  $N \times 1$ , denoted:

$$y_A = f(A) \quad y_B = f(B) \quad y_{C_j} = f(C_j) \quad (\text{A.1})$$

With  $f$  being considered as the application of the combination of the FEM model 2.2.2 and the calculation of the equivalent Young's modulus of the membrane 2.2.3.

These sets of permutations will enable us to calculate the first-order sensitivity indices and the total sensitivity indices using the following formulae:

$$S_j = \frac{\frac{1}{N} \sum_{i=1}^N y_A^{(i)} y_{C_i}^{(i)} - f_0^2}{\frac{1}{N} \sum_{i=1}^N (y_A^{(i)})^2 - f_0^2} \quad (\text{A.2})$$

$$S_{T_j} = 1 - \frac{\frac{1}{N} \sum_{i=1}^N y_B^{(i)} y_{C_i}^{(i)} - f_0^2}{\frac{1}{N} \sum_{i=1}^N (y_A^{(i)})^2 - f_0^2} \quad (\text{A.3})$$

With  $f_0$  being the average of  $y_A$ :

$$f_0 = \frac{1}{N} \sum_{i=1}^N y_A^{(i)} \quad (\text{A.4})$$

Using the formulae (A.2) and (A.3), we obtain coefficients between 0 and 1 that allow us to determine the importance of an input variable in relation to an output variable in a model. The first-order sensitivity indices  $S_j$  give an indication of the importance of the  $j$  variables only, while the total sensitivity indices  $S_{T_j}$  give an indication of the  $j$  variables as well as their interactions with the other variables.

## B metamodel parameters

Parameters	Estimations	Std. Error
(Intercept)	-4.4010e+00	1.7930e-02
pl	-3.9988e-02	2.4261e-03
pw	-3.7714e-01	2.8068e-03
fw	1.3872e+00	2.3438e-02
ym	9.7424e-06	5.5332e-08
pl <sup>2</sup>	2.3758e-03	2.2328e-04
pw <sup>2</sup>	1.5031e-02	2.2262e-04
fw <sup>2</sup>	-3.6363e-01	8.9276e-03
ym <sup>2</sup>	-9.7935e-12	9.8190e-14
pw:fw	3.8417e-02	1.2247e-03

**Table 3.** Table of the metamodel parameters

## References

- [1] C. E. Varela, Y. Fan, and E. T. Roche, “Optimizing Epicardial Restraint and Reinforcement Following Myocardial Infarction: Moving Towards Localized, Biomimetic, and Multitherapeutic Options,” *Biomimetics*, vol. 4, p. 7, Mar. 2019. Number: 1 Publisher: Multidisciplinary Digital Publishing Institute.
- [2] K. Thygesen, J. S. Alpert, A. S. Jaffe, B. R. Chaitman, J. J. Bax, D. A. Morrow, H. D. White, ESC Scientific Document Group, K. Thygesen, J. S. Alpert, A. S. Jaffe, B. R. Chaitman, J. J. Bax, D. A. Morrow, H. D. White, H. Mickley, F. Crea, F. Van de Werf, C. Bucciarelli-Ducci, H. A. Katus, F. J. Pinto, E. M. Antman, C. W. Hamm, R. De Caterina, J. L. Januzzi, F. S. Apple, M. A. Alonso Garcia, S. R. Underwood, J. M. Canty, A. R. Lyon, P. J. Devereaux, J. L. Zamorano, B. Lindahl, W. S. Weintraub, L. K. Newby, R. Virmani, P. Vranckx, D. Cutlip, R. J. Gibbons, S. C. Smith, D. Atar, R. V. Luepker, R. M. Robertson, R. O. Bonow, P. G. Steg, P. T. O’Gara, K. A. A. Fox, D. Hasdai, V. Aboyans, S. Achenbach, S. Agewall, T. Alexander, A. Avezum, E. Barbato, J.-P. Bassand, E. Bates, J. A. Bittl, G. Breithardt, H. Bueno, R. Bugiardini, M. G. Cohen, G. Dangas, J. A. de Lemos, V. Delgado, G. Filippatos, E. Fry, C. B. Granger, S. Halvorsen, M. A. Hlatky, B. Ibanez, S. James, A. Kastrati, C. Leclercq, K. W. Mahaffey, L. Mehta, C. Müller, C. Patrono, M. F. Piepoli, D. Piñero, M. Roffi, A. Rubboli, S. Sharma, I. A. Simpson, M. Tendera, M. Valgimigli, A. C. van der Wal, S. Windecker, M. Chettibi, H. Hayrapetyan, F. X. Roithinger, F. Aliyev, V. Sujayeva, M. J. Claeys, E. Smajić, P. Kala, K. K. Iversen, E. El Hefny, T. Marandi, P. Porela, S. Antov, M. Gilard, S. Blankenberg, P. Davlouros, T. Gudnason, R. Alcalai, F. Colivicchi, S. Elezi, G. Baitova, I. Zakke, O. Gustiene, J. Beissel, P. Dingli, A. Grosu, P. Damman, V. Juliebø, J. Legutko, J. Morais, G. Tatu-Chitoiu, A. Yakovlev, M. Zavatta, M. Nedeljkovic, P. Radsel, A. Sionis, T. Jernberg, C. Müller, L. Abid, A. Abaci, A. Parkhomenko, and S. Corbett, “Fourth universal definition of myocardial infarction (2018),” *European Heart Journal*, vol. 40, pp. 237–269, Jan. 2019.

- [3] I. Zlatanova, “Macrophages, inflammation et réparation cardiaque,”
- [4] S. A. Clarke, R. K. Ghanta, G. Ailawadi, and J. W. Holmes, “Cardiac restraint and support following myocardial infarction,” in *Cardiovascular and cardiac therapeutic devices*, pp. 169–206, Springer, 2013.
- [5] K. D. Dwyer and K. L. Coulombe, “Cardiac mechanostructure: using mechanics and anisotropy as inspiration for developing epicardial therapies in treating myocardial infarction,” *Bioactive Materials*, vol. 6, no. 7, pp. 2198–2220, 2021.
- [6] M. H. Kwon, M. Cevasco, J. D. Schmitto, and F. Y. Chen, “Ventricular restraint therapy for heart failure: A review, summary of state of the art, and future directions,” *The Journal of Thoracic and Cardiovascular Surgery*, vol. 144, pp. 771–777.e1, Oct. 2012.
- [7] S. Nakatani, “Left Ventricular Rotation and Twist: Why Should We Learn?,” *Journal of Cardiovascular Ultrasound*, vol. 19, no. 1, p. 1, 2011.
- [8] J.-P. Jehl, P. Dan, A. Voignier, N. Tran, T. Bastogne, P. Maureira, and F. Cleymand, “Transverse isotropic modelling of left-ventricle passive filling: mechanical characterization for epicardial biomaterial manufacturing,” *Journal of the mechanical behavior of biomedical materials*, vol. 119, p. 104492, 2021.
- [9] R. Emig, C. M. Zgierski-Johnston, V. Timmermann, A. J. Taberner, M. P. Nash, P. Kohl, and R. Peyronnet, “Passive myocardial mechanical properties: meaning, measurement, models,” *Biophysical Reviews*, vol. 13, pp. 587–610, Oct. 2021.
- [10] G. C. Engelmayer, M. Cheng, C. J. Bettinger, J. T. Borenstein, R. Langer, and L. E. Freed, “Accordion-like honeycombs for tissue engineering of cardiac anisotropy,” *Nature materials*, vol. 7, no. 12, pp. 1003–1010, 2008.
- [11] A. Sionkowska, “Current research on the blends of natural and synthetic polymers as new biomaterials: Review,” *Progress in Polymer Science*, vol. 36, pp. 1254–1276, Sept. 2011.
- [12] X. Lin, Y. Liu, A. Bai, H. Cai, Y. Bai, W. Jiang, H. Yang, X. Wang, L. Yang, N. Sun, and H. Gao, “A viscoelastic adhesive epicardial patch for treating myocardial infarction,” *Nature Biomedical Engineering*, vol. 3, pp. 632–643, Apr. 2019.
- [13] E. A. Ovcharenko, K. U. Klyshnikov, M. A. Rezvova, L. V. Antonova, T. V. Glushkova, S. E. Vinokurov, V. V. Sevostyanova, E. O. Krivkina, A. V. Batranin, Y. N. Zakharov, V. G. Borisov, Y. A. Kudryavtseva, and L. S. Barbarash, “Analysis of the Flexural Rigidity of Vascular Grafts by Numerical Simulation Methods,” *Biophysics*, vol. 64, pp. 485–492, May 2019.
- [14] M. Ravandi, A. Moradi, S. Ahlquist, and M. Banu, “Numerical Simulation of the Mechanical Behavior of a Weft-Knitted Carbon Fiber Composite under Tensile Loading,” *Polymers*, vol. 14, p. 451, Jan. 2022.

- [15] A. Poerio, B. Guibert, M. M. Leroux, J. F. Mano, F. Cleymand, and J.-P. Jehl, “Mechanical characterization of 3d-printed patterned membranes for cardiac tissue engineering: An experimental and numerical study,” *Biomedicines*, vol. 11, no. 3, 2023.
- [16] COMSOL AB, “Comsol multiphysics®.”
- [17] T. M. Inc., “Matlab version: 9.13.0 (r2022b),” 2022.
- [18] Y. Zhang, W. Mu, Y. Zhang, X. He, Y. Wang, H. Ma, T. Zhu, A. Li, Q. Hou, W. Yang, Y. Ding, S. Ramakrishna, and H. Li, “Recent advances in cardiac patches: Materials, preparations, and properties,” *ACS Biomaterials Science & Engineering*, vol. 8, no. 9, pp. 3659–3675, 2022. PMID: 36037313.
- [19] *COMSOL Multiphysics: Structural mechanics module. User’s guide.* Comsol, 2022.
- [20] D. K. Lin, T. W. Simpson, and W. Chen, “Sampling strategies for computer experiments: design and analysis,” *International Journal of Reliability and applications*, vol. 2, no. 3, pp. 209–240, 2001.
- [21] J. Santiago, M. Claeys-Bruno, and M. Sergent, “Construction of space-filling designs using wsp algorithm for high dimensional spaces,” *Chemometrics and Intelligent Laboratory Systems*, vol. 113, pp. 26–31, 2012.
- [22] V. R. Joseph, “Space-filling designs for computer experiments: A review,” *Quality Engineering*, vol. 28, no. 1, pp. 28–35, 2016.
- [23] S. S. Garud, I. A. Karimi, and M. Kraft, “Design of computer experiments: A review,” *Computers & Chemical Engineering*, vol. 106, pp. 71–95, 2017.
- [24] A. Saltelli, ed., *Global sensitivity analysis: the primer.* Chichester, England ; Hoboken, NJ: John Wiley, 2008. OCLC: ocn180852094.
- [25] I. M. Sobol’, “ON THE DISTRIBUTION OF POINTS IN A CUBE AND THE APPROXIMATE EVALUATION OF INTEGRALS,”
- [26] I. Sobol, “Uniformly distributed sequences with an additional uniform property,” *USSR Computational Mathematics and Mathematical Physics*, vol. 16, pp. 236–242, Jan. 1976.
- [27] A. Saltelli, “Making best use of model evaluations to compute sensitivity indices,” *Computer Physics Communications*, 2002.
- [28] I. M. Sobol’, “Sensitivity estimates for nonlinear mathematical models,” vol. 2, p. 112–118, Dec 1990.
- [29] T. Homma and A. Saltelli, “Importance measures in global sensitivity analysis of nonlinear models,” *Reliability Engineering & System Safety*, vol. 52, pp. 1–17, Apr. 1996.
- [30] R. Genuer and J.-M. Poggi, “Arbres CART et Forêts aléatoires, Importance et sélection de variables,”

- [31] B. P. Lovatti, M. H. Nascimento, Á. C. Neto, E. V. Castro, and P. R. Filgueiras, “Use of random forest in the identification of important variables,” *Microchemical Journal*, vol. 145, pp. 1129–1134, 2019.
- [32] G. A. Lewis, D. Mathieu, and R. Phan-Tan-Luu, *Pharmaceutical Experimental Design*. Marcel Dekker, 2005.
- [33] T. Morgan-Wall, *spacefillr: Space-Filling Random and Quasi-Random Sequences*, 2022. R package version 0.3.2.